Boundary Integral Solution of Quasi-linear Laplace Equation

Jian Ding* and Wenjing Ye**

Woodruff School of Mechanical Engineering, Georgia Institute of Technology
771 Ferst Dr., Love 316, Atlanta, GA 30332, USA
*gte731s@prism.gatech.edu, **wenjing.ye@me.gatech.edu

ABSTRACT

For non-homogeneous or nonlinear problems, a major difficulty in applying the Boundary Element Method is the treatment of the volume integrals that arise. A recent proposed method, the grid-based integration method (GIM), uses a 3D uniform grid to efficiently perform volume integration. The efficiency of the GIM has been demonstrated on 3D Poisson problems. In this paper, we report our work on the extension of this technique to quasilinear problems. Numerical results of a 3D Helmholtz problem and a quasilinear Laplace problem on a solid sphere domain and a multiply-connected domain with Dirichlet boundary conditions are compared with analytic solutions. The performance of the GIM is measured by plotting the L_2-norm error as a function of the overall CPU time and is compared with the auxiliary domain method in the Helmholtz problem.

Keywords: Quasilinear equation, BEM, volume integral, precorrected-FFT technique, grid-based integration method.

1. INTRODUCTION

The Boundary Element Method (BEM) has been established as a powerful numerical method for solving a large variety of engineering problems particularly those with complex 3-D geometries. It is, however, true that to date most applications of the BEM are limited to linear and homogeneous problems. A major difficulty in applying the BEM to nonlinear or nonhomogeneous problems is the treatment of the volume integrals that arise in the boundary integral formulation. The existing approaches can be classified into two categories: meshless methods such as DRM [1] and cell based direct integration schemes [2,5]. Meshless methods use different techniques to either eliminate the volume integrals or (approximately) transform them into boundary integrals. The major advantage of this type of methods is that the boundary only nature of the BEM is retained. However, the quality of these methods depends on the quality of the radial basis functions (RBF) approximation. Finding the optimal methods for approximations is still an active research topic. Cell-based direct integration schemes employ an interior volume mesh to directly perform the integration. A major advantage of this type of schemes is the high accuracy. However, a disadvantage of cell-based direct integration schemes is the requirement of volume discretization of the interior problem domain.

The grid-based integration method (GIM), recently proposed and presented in [3], is similar to cell-based direct integration schemes in terms of that the volume integration is performed directly. The volume integral that contains the nonlinear term is evaluated directly with the aid of the 3D uniform grid constructed initially for the acceleration of surface integration [4]. This grid is also used to accelerate volume integration to further reduce the computational cost [3]. Successful applications of the GIM have been demonstrated previously on 3-D Poisson problems [3]. In this paper, we present new developments and results on the extension of the grid-based approach to 3-D quasilinear problems.

2. PROBLEM FORMULATION

The equations considered in this work are quasilinear equations, which have the form of

$$Lu = f(u, \mathbf{x}) . \tag{1}$$

In (1), L denotes a linear operator, u is the unknown, $\mathbf{x}$ is the spatial variable and f is a nonlinear function of u.

Assuming the fundamental solution (Green's function) corresponding to the linear operator, L, exists and is available, and regarding the nonlinear function, f, as a pseudo body force, an integral formulation of Eq. (1) can be formed based on the Green's function of the linear operator. In the case of quasilinear Laplace problems, this integral formulation reads

$$c(\mathbf{x})u(\mathbf{x}) + \int_{\partial\Omega}^{CPV} \frac{\partial G(\mathbf{x},\mathbf{y})}{\partial n(\mathbf{y})} u(\mathbf{y}) dS(\mathbf{y}) - \int_{\partial\Omega} G(\mathbf{x},\mathbf{y}) \frac{\partial u(\mathbf{y})}{\partial n(\mathbf{y})} dS(\mathbf{y})$$
$$= -\int_{\Omega} G(\mathbf{x},\mathbf{y}) f(u(\mathbf{y}),\mathbf{y}) dV(\mathbf{y}), \tag{2}$$

where $c(\mathbf{x})$ is the self-term and CPV indicates the Cauchy principal value of the integral. In (2), Ω is the domain of the problem with boundary $\partial\Omega$, $n(\mathbf{y})$ is the unit outward normal vector at the field point $\mathbf{y}$, $\mathbf{x}$ is the evaluation point and $G(\mathbf{x},\mathbf{y})$ is the Green's function of the Laplace operator.

A key step in the grid-based integration method is to transfer the volume integral, e.g., the right-hand side in Eq. (2), evaluated on the problem domain Ω into a volume integral evaluated on a regular 3-D grid, *B*. This grid, as shown in Figure 1, consists of a set of cubes and is the same grid used to accelerate surface integration [3]. Mathematically, this step can be represented as

$$\int_{\Omega} G(\mathbf{x},\mathbf{y}) f(u(\mathbf{y}),\mathbf{y}) dV(\mathbf{y}) = \int_{B} G(\mathbf{x},\mathbf{y}) \tilde{f}(u(\mathbf{y}),\mathbf{y}) dV(\mathbf{y}), \quad (3)$$

where $\tilde{f}(u(\mathbf{y}),\mathbf{y}) = f(u(\mathbf{y}),\mathbf{y})$ if $\mathbf{y} \in \Omega$ and $\tilde{f}(u(\mathbf{y}),\mathbf{y}) = 0$ if $\mathbf{y} \in B \backslash \Omega$, $B = \sum_i C_i$ denotes the uniform 3-D grid and C_i is the *i*th cube. By doing so, we have partitioned the volume-integration domain into two regions: the interior and the boundary regions. The cubes in the interior region fully coincide with the problem domain while the cubes in the boundary region intersect with the problem domain.

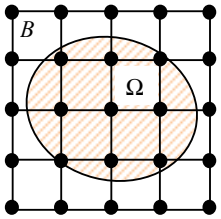

Figure 1. 2-D illustration of the problem domain (Ω, shaded area) and the uniform grid (*B*). The interior region consists of four squares located at the center of the grid. The rest forms the boundary region.

Combining Eqs. (2) and (3), the integral formulation of Eq. (1) is

$$c(\mathbf{x})u(\mathbf{x}) + \int_{\partial\Omega}^{CPV} \frac{\partial G(\mathbf{x},\mathbf{y})}{\partial n(\mathbf{y})} u(\mathbf{y}) dS(\mathbf{y}) - \int_{\partial\Omega} G(\mathbf{x},\mathbf{y}) \frac{\partial u(\mathbf{y})}{\partial n(\mathbf{y})} dS(\mathbf{y})$$
$$= -\sum_i \int_{C_i} G(\mathbf{x},\mathbf{y}) \tilde{f}(u(\mathbf{y}),\mathbf{y}) dV(\mathbf{y}). \quad (4)$$

3. SOLUTION SCHEMES

Due to the dependence of function $\tilde{f}$ on *u*, a successive-substitution iteration scheme is employed to solve Eq. (4). At the beginning of the iteration, the interior value of *u* is assumed. The volume integrals are then evaluated and the integral equation is solved to find the unknowns at the boundary using the standard boundary element method combined with the precorrected-FFT acceleration technique [4]. The obtained boundary values together with the given boundary conditions are then used to update interior value of *u* and iteration continues until a convergence criterion is met. In this work, zero initial values for *u* at interior points are used and the convergence criterion employed is that the difference, measured in L_2-norm, between the boundary unknowns obtained from the latest two iterations must be less than or equal to a pre-set tolerance.

A major step in the implementation, the evaluation of volume integrals on a set of cubes, follows the schemes discussed in Ref. [3]. For interior region, Gaussian Quadrature is employed directly for the evaluation of nonsingular integrals on each cube. The integration accuracy depends on the order of Gaussian Quadrature and the smoothness of function *u* within the cube. For boundary region, the "projection + transformation" scheme is used to first discretize the integration domain within each cube into a set of prisms based on the surface panels as shown in Figure 2.

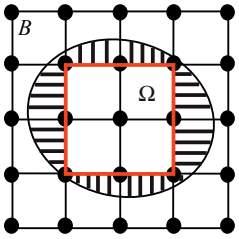

Figure 2. Volume elements used in the evaluation of volume integrals: cubes in the interior region and prisms in the boundary region.

These prisms are then mapped into a regular domain and integration is performed using Gaussian Quadrature for non-singular integrals. For singular surface integrals, an additional coordinate transformation whose Jacobian cancels the singularity is performed before Gaussian Quadrature is applied. For the evaluation of singular volume integrals, the integral is split into two as shown in Eq. (5).

$$\int_{C_i} G(\mathbf{x},\mathbf{y}) \tilde{f}(u(\mathbf{y}),\mathbf{y}) dV(\mathbf{y}) = \int_{C_i} G(\mathbf{x},\mathbf{y}) \left[\tilde{f}(u(\mathbf{y}),\mathbf{y}) - \tilde{f}(u(\mathbf{x}),\mathbf{x}) \right] dV(\mathbf{y})$$
$$+ \tilde{f}(u(\mathbf{x}),\mathbf{x}) \int_{C_i} G(\mathbf{x},\mathbf{y}) dV(\mathbf{y}). \quad (5)$$

The first integral in Eq. (5) is no longer singular and regular Gaussian Quadrature can then be applied. To evaluate the second integral, a subdivision of the integration domain, a prism or a cube, is performed to form a set of prisms with the singular point located on one of their vertices. The Jacobian cancellation technique is then applied to remove the singularity. On theory, this approach can be applied directly to evaluate $\int_{C_i} G(\mathbf{x},\mathbf{y}) \tilde{f}(u(\mathbf{y}),\mathbf{y}) dV(\mathbf{y})$. However, this requires the evaluation of function $\tilde{f}$ at additional Gauss points, while in $\int_{C_i} G(\mathbf{x},\mathbf{y}) dV(\mathbf{y})$, the function $\tilde{f}$ is one at any point inside the integration domain.

The acceleration schemes for both surface and volume integrals are based on the precorrected-FFT technique and detailed discussion can be found in references [3,4].

4. RESULTS AND DISCUSSION

Two examples, a nonhomogeneous Helmholtz problem and a quasilinear Laplace problem, are presented in this section. In both problems, Dirichlet boundary conditions are prescribed. Two domains (Fig. 3), a solid sphere (centered at origin with radius 1) and a multiply-connected domain, i.e., a solid ellipsoid ($a = c = \sqrt{2}$, b=2, centered at origin) with two spherical exclusions (r =0.5, centered at (0,±1,0)), are considered. The dimensions of domain 2 are chosen so that our problem domain is as close as that of Hsiao's [5]. Three successively refined discretizations starting with 192 panels for the ellipsoid and 48 panels for each sphere are used for the multiply-connected domain.

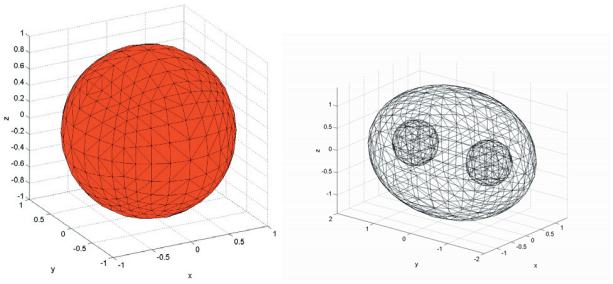

(a) (b)

Figure 3. Problem domains: (a) Domain 1: a solid sphere, (b) Domain 2: a solid ellipsoid domain with two spherical exclusions.

Example 1: Helmholtz equation

The governing equation for this problem is

$$\nabla^2 u = -u + h(x, y, z), \tag{6}$$

with $h = 4x^2 + 4y^2 + 12xy + 3x^3 y + 2x^2 y^2 - xy^3 + z$.

This equation has been solved on a parallelepiped with two spherical exclusions by Hsiao *et al.* using the dual reciprocity method, the auxiliary domain method and the classical domain integration method. A careful comparison on the performances of these methods has been performed and is given in [5]. It has been found that the auxiliary domain method (ADM) is the most efficient. Thus results obtained from the ADM will be used for performance comparison in this paper.

An analytic solution to Eq. (6), same as that in [5], $u = 3x^3 y + 2x^2 y^2 - xy^3 + z$, is used to prescribe the boundary conditions. The equation is solved using the grid-based integration method described in sections 2 and 3. The normal flux, $q = \partial u / \partial n$, at the boundaries and the interior values of u are calculated and compared with analytic solutions. The corresponding L_2-norm errors at different discretizations of two domains are presented in Tables 2 and 3. It is clear from the tables that the convergence rate of q is of $O(h)$, where h is the size of the surface element. This is not surprising since the accuracy of q is largely controlled by the surface discretization provided that the volume term is computed reasonably accurately. The accuracy of u, however, depends not only on the surface mesh but also on "volume elements", i.e., the number of interior cubes and the number of prisms in the boundary region for a given order of Gaussian Quadrature. It is possible to reduce errors by increasing the number of cubes per side while maintaining the same surface mesh. For example, in the case of 3072 surface panels on domain 1, the L_2-norm error of u reduces from 4.99% to 2.69% when the number of cubes per side increases from 6 to 8. This attribute, which could be advantageous in certain cases, is due to the relative independence between surface mesh and the grid in this approach.

Table 2. L_2-norm error for Helmholtz problem on domain 1

Number of surface panels	# of cubes per side	L_2-norm error for q	L_2-norm error for u
48	6	9.36%	23.04%
192	6	6.93%	11.79%
768	6	2.93%	6.44%
3072	8	1.92%	2.69%

Table 3. L_2-norm error for Helmholtz problem on domain 2

Number of surface panels	# of cubes per side	L_2-norm error for q	L_2-norm error for u
288	4	12.86%	28.80%
1152	8	4.21%	8.64%
4608	16	2.20%	3.81%

Adopting the performance measure used in Hsiao *et al.* [5], the L_2-norm error of q on domain 2 at difference discretizations are plotted as a function of the overall CPU time in Fig. 4. The tolerance used for convergence is 10^{-3}. The number of iterations required to achieve convergence is three in all cases. Smaller tolerances, such as 10^{-4} and 10^{-5}, have been used which yield essentially the same accuracy.

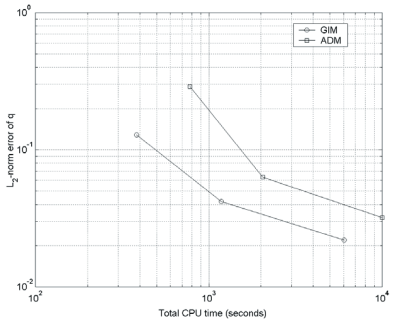

Figure 4. L_2-norm error of q as a function of the overall CPU time for Helmholtz problem on domain 2.

Also shown in Figure 4 are the results obtained from the ADM [5].Although it is difficult to directly compare the performances of the two approaches based on these results due to the differences in the two simulations, for example, different type of boundary conditions and different computers (A PC with Pentium 4 CPU, 1.8GHz and 1.5 GB of RAM is used in this work), the accuracy and efficiency of the grid-based integration method is nevertheless clearly demonstrated.

Example 2: Quasi-linear Laplace equation

The governing equation for this problem is

$$\Delta u = u + u^3 . \tag{7}$$

This example is chosen because an analytic solution, $u = \tan((x + y + z)/\sqrt{6})$, can be readily obtained. Again, the analytic solution of u is used to prescribe the boundary conditions. The same two problem domains as those of the Helmholtz problem shown in Figure 3 and same surface discretizations are used. However, only results for the multiply-connected domain are presented due to limited space.

Table 4 shows L_2-norm errors for both q and u as compared with the analytic solutions at different discretizations. Again, $O(h)$ convergence rate is observed.

Table 4. L_2-norm error for quasi-linear Laplace problem on domain 2

Number of surface panels	# of cubes per side	L_2-norm error for q	L_2-norm error for u
288	4	6.24%	48.48%
1152	8	3.57%	4.04%
4608	16	1.70%	2.58%

The performance of the GIM in this problem is comparable to that in the Helmholtz problem. Figure 5 shows the plot of L_2-norm error of q versus the overall CPU time on domain 2. The number of iterations needed to achieve a convergence with a tolerance of 10^{-3} is greater than that in the Helmholtz problem. It took six iterations for the successive-substitution iteration scheme to converge in the first two cases and five in the last case as compared with three in the Helmholtz problem. This is somewhat expected since in general nonlinear problems, if they converge, require more iterations than linear ones.

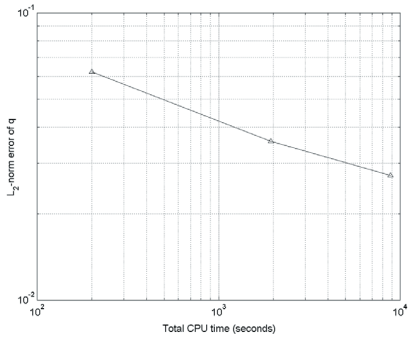

Figure 5. L_2-norm error of q as a function of the overall CPU time for quasi-linear Laplace problem on domain 2.

5. CONCLUSIONS

In this paper, the grid-based integration method has been extended to solve quasilinear problems. Numerical results of a 3D Helmholtz problem and a quasilinear Laplace problem on a solid sphere domain and a multiply-connected domain with Dirichlet boundary conditions are presented. These results are compared with analytic solutions and O(h) convergence rate is achieved.

The performance of the GIM in the Helmholtz problem is compared with the ADM, a method that over performs the DRM and the classical direct integration method in this problem, by using the approach of plotting the L_2-norm error as a function of the overall CPU time. Although it is difficult to directly draw a conclusion of which method performs better, due to the differences in the two simulations, the favorable comparison has clearly indicated the efficiency of the GIM. The performance of the GIM in the nonlinear case is comparable to that in the Helmholtz problem, although the number of iterations required to achieve convergence is larger in the nonlinear case.

REFERENCES

[1] Partridge PW, Brebbia CA and Wrobel LC, *The Dual Reciprocity Boundary Element Method*. Elsevier, London, 1992.

[2] Ingber MS, Mammoli A and Brown M, A Comparison of Domain Integral Evaluation Techniques for Boundary Element Methods, *IJNME*, 2001; **52**(4): 417-432.

[3] Jian Ding, Wenjing Ye, and Leonard Gray, An Accelerated Surface Discretization Based BEM Approach for Non-Homogeneous Linear Problems in 3-D Complex Domains, *IJNME*, in press.

[4] Phillips, J. R. and White, J., *IEEE Trans. On CAD* 1997; **16(10)**: 1059 – 1072.

[5] Hsiao SC, Mammoli AA and Ingber MS, *Computational Mechanics*, 2003; **32**: 226-233.